Organic & Biomolecular Chemistry

ROYAL SOCIETY OF CHEMISTRY

PAPER

View Article Online
View Journal

Cite this: DOI: 10.1039/d0ob01586e

Deciphering the chemical instability of sphaeropsidin A under physiological conditions – degradation studies and structural elucidation of the major metabolite†

Alet E. van der Westhuyzen,[a] Aude Ingels,[b,c] Rémi Rosière,[b] Karim Amighi,[b] Lukas Oberer,[d] Kirk R. Gustafson,[e] Dongdong Wang,[e] Antonio Evidente,[f] Lucia Maddau,[g] Marco Masi,[f] André de Villiers,[a] Ivan R. Green,[a] Walter Berger,[h] Alexander Kornienko,[i] Veronique Mathieu*[b,c] and Willem A. L. van Otterlo*[a]

Received 31st July 2020,
Accepted 21st September 2020

DOI: 10.1039/d0ob01586e

rsc.li/obc

The fungal metabolite sphaeropsidin A (SphA) has been recognised for its promising cytotoxicity, particularly towards apoptosis- and multidrug-resistant cancers. Owing to its intriguing activity, the development of SphA as a potential anticancer agent has been pursued. However, this endeavour is compromised since SphA exhibits poor physicochemical stability under physiological conditions. Herein, SphA's instability in biological media was explored utilizing LC-MS. Notably, the degradation tendency was found to be markedly enhanced in the presence of amino acids in the cell medium utilized. Furthermore, the study investigated the presence of degradation adducts, including the identification, isolation and structural elucidation of a major degradation metabolite, (4*R*)-4,4′,4′-trimethyl-3′-oxo-4-vinyl-4′,5′,6′,7′-tetrahydro-3′*H*-spiro[cyclohexane-1,1′-isobenzofuran]-2-ene-2-carboxylic acid. Considering the reduced cytotoxic potency of aged SphA solutions, as well as that of the isolated degradation metabolite, the reported antiproliferative activity has been attributed primarily to the parent compound (SphA) and not its degradation species. The fact that SphA continues to exhibit remarkable bioactivity, despite being susceptible to degradation, motivates future research efforts to address the challenges associated with this instability impediment.

Introduction

Sphaeropsidins A–G (**1**–**7**, Fig. 1) are pimarane diterpenoids produced by several phytopathogenic fungi belonging to the genera *Sphaeropsis* and *Diplodia*.[1,2] While being notorious for inducing severe canker diseases of Mediterranean forest plants, the sphaeropsidins have received growing interest for their medicinal potential.[3–5] Amongst the group (**1**–**7**), sphaeropsidin A (**1**, SphA) has been recognised as the main bioactive member. To date, reported sources of SphA include species of *Diplodia* (*D. cupressi*, *D. corticola*, *D. quercivora*) and *Asperigillus* (*A. chevalieri*, *A. candidus*).[6–8] Apart from the attractive phytotoxic, antimicrobial and insecticidal activities, SphA has been noted for its intriguing cytotoxicity, particularly towards apoptosis- and multidrug-resistant cancers.[9–12] Apoptosis-resistant cancers represent a major challenge in the clinic.[13–17] Since the majority of chemotherapeutic drugs are aimed at the induction of apoptosis in cancer cells, resistance of this sort generally leads to poor treatment outcomes.[18–20] For this reason, the discovery and recognition of agents capable of

[a]*Department of Chemistry and Polymer Science, University of Stellenbosch, Matieland, 7600 Stellenbosch, Western Cape, South Africa. E-mail: wvo@sun.ac.za*
[b]*Department of Pharmacotherapy and Pharmaceutics, Université libre de Bruxelles (ULB), Boulevard du Triomphe, Accès 2, 1050 Ixelles, Belgium. E-mail: Veronique.Mathieu@ulb.be*
[c]*ULB Cancer Research Center, Université libre de Bruxelles (ULB), 1050 Bruxelles, Belgium*
[d]*Novartis Institutes for BioMedical Research, Global Discovery Chemistry, Basel, Switzerland*
[e]*Molecular Targets Program, Center for Cancer Research, National Cancer Institute, Frederick, Maryland 21702-1201, USA*
[f]*Department of Chemical Sciences, University of Naples Federico II, Complesso Universitario Monte S. Angelo, Via Cintia 4, 80126 Naples, Italy*
[g]*Department of Agriculture, Section of Plant Pathology and Entomology, University of Sassari, Viale Italia 39, 07100 Sassari, Italy*
[h]*Department of Medicine I, Institute of Cancer Research and Comprehensive Cancer Center, Medical University of Vienna, Vienna, Austria*
[i]*Department of Chemistry and Biochemistry, Texas State University, San Marcos, Texas 78666, USA*

†Electronic supplementary information (ESI) available. See DOI: 10.1039/d0ob01586e

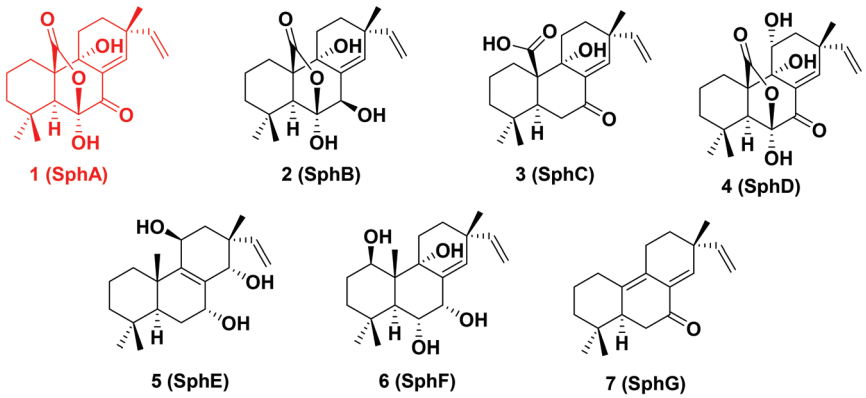

Fig. 1 Chemical structures of sphaeropsidins A–G (**1–7**).

overcoming such malignancies is potentially of significant value.

The antiproliferative activity of SphA towards cancer cells was first noted in 2011 by Wang *et al.*[21] In the following year, we reported on our findings of low micromolar growth-inhibitory IC_{50} values of SphA against several cancer cell lines, with the natural product being as/or more potent *in vitro* than various conventional chemotherapeutic drugs.[4] Further, the investigations of the effects of this compound against the National Cancer Institute (NCI) panel of 60 human cancer cell lines revealed melanoma and kidney cancer subpanels were more sensitive to the cytotoxic effects of SphA (lower LC_{50} values).[12] Moreover, the NCI COMPARE data analyses revealed that SphA displays a unique sensitivity profile, unmatched by any other agent in the 763 000 compound database with a correlation coefficient of >0.7.[12] Another attractive feature exhibited by SphA was its ability to overcome various forms of cancer drug resistance, including those related to multi-drug ABC transporter expression, *e.g.* ABCB1 (P glycoprotein), ABCG2 (breast cancer resistance protein) or MVP (Major Vault Protein).[12] An encouraging finding was also the fact that several normal cells, *i.e.* HUVEC and normal melanocytes were less sensitive to SphA, which serves as further motivation towards its development as a potential anticancer agent.[12] The interesting cytotoxicity features displayed by SphA have been further ascribed, at least partly to its ability to impair the regulatory volume increase (RVI) process, leading to perturbation of the cellular ion homeostasis. These effects were found to lead to marked and rapid cell shrinkage directly triggering apoptosis and overcoming cell death resistance.[12]

Based on the promising bioactivity displayed by SphA, together with the poor prognosis of advanced melanoma, a recent study investigated *in vitro* chemocombinations of SphA with conventional pro-apoptotic chemotherapeutic agents.[22] This revealed that SphA combinations with cisplatin or temozolomide increased their *in vitro* potency in a synergistic manner.

Despite these promising anticancer properties, the potential development of SphA is unfortunately thwarted as a result of its poor physicochemical stability under physiological conditions. This impediment was first reported by Lallemand *et al.* in a preliminary degradation investigation which explored the stability of SphA in cell culture medium at physiological pH.[4] From this quantitative analysis, it was noted that approximately 32–43% of SphA was degraded within 24 h of incubation in cell culture medium. This unappealing feature could result in an unpredictable toxicological profile of SphA as well as inefficient *in vivo* drug delivery. Consequently, the instability associated with SphA raises concern with regard to the actual active species that may well be one of the SphA metabolites.

To provide a solid foundation for a possible pharmaceutical development of SphA, the issue of instability requires immediate attention. To this end, the primary focus of this study was to evaluate the extent of degradation of SphA as well as identify and elucidate the structure(s) of any major decomposition metabolites that may contribute to its intriguing antiproliferative activity.

Results and discussion

The layout of this manuscript follows initial degradation analysis of SphA incubated and monitored in MEM cell culture medium or PBS buffer solution at both room temperature and 37 °C, along with maximal solubility determination. Subsequent degradation studies of SphA were then conducted in parallel with anti-cancer activity evaluation, gaining insight with respect to the *in vitro* activity of SphA's degradation metabolites. Augmenting these results, a more in-depth analysis of SphA's degradation behaviour and a deciphering of its degradation metabolites was undertaken utilizing LC-MS. Moreover, the instability of SphA was further explored by studying its anti-cancer activity in the presence/absence of *N*-acetylcysteine (NAC). Finally, the investigation led to the isolation, structural elucidation and biotesting of a major SphA degradation metabolite.

Solubility and stability analyses of SphA in phosphate buffer

The aqueous solubility of a therapeutic candidate is a key physicochemical property, considering that it directly impacts the maximum drug dose which can be absorbed.[23,24] It is therefore crucial that any solubility liabilities are identified during early stages of drug development.[25,26] The maximal SphA solubility evaluated in PBS reached 1.124 ± 0.001 mg mL^{-1} in PBS at pH 7.4 and room temperature (20–22 °C). From the stability analysis results, degradation of SphA was limited in PBS at room temperature, ~5% within 48 h, whereas the degradation was found to be greater in MEM (which contains a cocktail of amino acids), reaching ~30% within 48 h (Fig. 2). On the other hand, degradation of SphA increased to ~80% and ~20% at 37 °C in cell culture medium and PBS respectively within 48 h (Fig. 2) and this data confirmed our previous observations.[4]

Parallel investigation of SphA degradation in culture medium and its residual anti-cancer activity

According to this rapid degradation of SphA in culture medium,[4] interest was aimed at determining whether degradation compound(s) could be partially responsible for SphA's anti-cancer activity *in vitro*. To address this question, we prepared a SphA stock solution in culture medium without serum that was further stored at 37 °C for a period of seven days. We acquired daily concentration–response curves on two melanoma cell lines and two primary cultures by means of MTT assay with this solution, starting the assay from day 0 and continuing to day 7 after its preparation. Fig. 3 shows a progressive increase in the mean IC_{50} values determined on the four cell lines over time. Parallel investigation of the residual SphA concentration in the stock solution by a HPLC method adapted from Lallemand *et al.*[4] showed indeed a time-dependent degradation of SphA, but residual activity was still observed after 7 days, even if more than 90% of SphA was degraded. The results suggest that one or several degradation metabolites may still display individual or collective anti-cancer activity. However, it is important to note that in our previous study, we observed irreversible effects triggered in cancer cells within only 6 h of treatment with freshly prepared SphA.[12] At this time point, the residual SphA concentration exceeds 82% of its initial concentration. Altogether, these data suggest that SphA displays potent anti-cancer effects *in vitro* while its degradation metabolite(s) are either poorly active or that the active one(s) are produced in very low amounts.

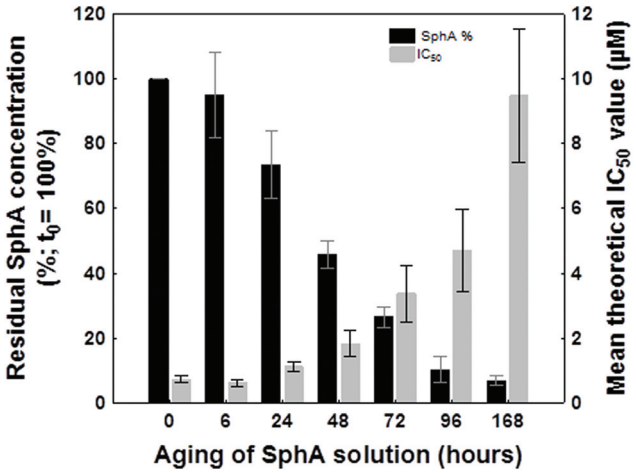

Fig. 3 Parallel evaluation of the anti-cancer activity of a SphA solution prepared in culture medium and stored at 37 °C before its use in the MTT assay and the residual SphA concentration. The MTT assay was conducted over 72 h of exposure to the "aged" SphA solutions. Data are presented as theoretical IC_{50} values expected if the SphA solution was stable over time (IC_{50} values were not corrected for the actual SphA concentration as measured by HPLC in order to highlight the possible effect of degradation products). IC_{50} data represent means ± SEM of IC_{50} data determined on 4 cell lines (B16F10, SK-MEL-28, VM21 and VM48). HPLC SphA data represent means ± SEM of three independent experiments.

SphA 1 degradation studies

The stability studies performed throughout the next steps of this investigation involved the incubation at 37 °C of SphA in various specified media, followed by the analysis of aliquots collected at different time intervals utilizing positive ion LC-ESI-MS. For clarity, it must be noted that SphA was identified by its molecular ion $[M + H]^+$ at *m/z* 347 ($C_{20}H_{27}O_5$) and base peak ions generally corresponding to a sodium adduct

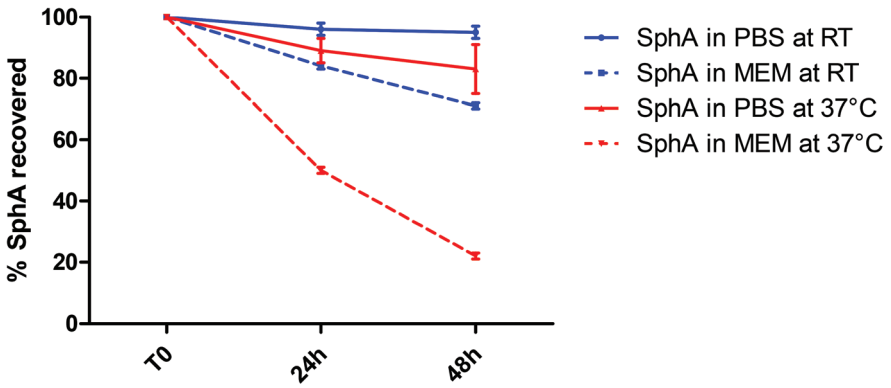

Fig. 2 Degradation of SphA in PBS and MEM at RT (20–22 °C) and at 37 °C. Data are presented as the mean % SphA recovered ± SD (*n* = 3).

$[M + Na]^+$ at *m/z* 369 ($C_{20}H_{26}O_5Na$) or a dehydrated molecular ion at *m/z* 329 ($C_{20}H_{25}O_4$), indicating facile loss of water $[M + H - H_2O]^+$ during the ionization process.

A first study of SphA's degradation behaviour conducted in H_2O/DMSO (9 : 1) revealed that, although predominately stable, the formation of two new putative species (**8** and **9**) at prolonged incubation periods was observed after 30 h. In fact, both **8** and **9** comprised two species, presumably isomers, which were separated chromatographically (see Fig. S1†). Since these SphA degradation derivatives were identified as minor metabolites throughout the investigation, initial attention was directed towards their formation. The total ion chromatogram (ESI positive) and HR-MS data of this experiment is presented in Fig. S1 and Table S1.† Accurate mass measurements of minor metabolites **8** and **9**, which correspond to *m/z* 301.1773 ($C_{19}H_{25}O_3$) and *m/z* 285.1852 ($C_{19}H_{25}O_2$), respectively, were consistent with the proposed degradation pathways involving lactone-bridge cleavage of SphA (Fig. 4). Compound **8** (*m/z* 301) has a mass difference of *m/z* 46 compared to SphA, while a loss of carbon dioxide (*m/z* 44) from the lactone bridge and water (*m/z* 18) possibly would give rise to metabolite **9** (*m/z* 285). The *m/z* 46 mass loss could be due to a number of possible fragmentations which include a proton-assisted loss of carbon monoxide[27] and water (shown as process **1** → **8** in Fig. 4, red arrows), a loss of CO_2 and H_2 (under oxidative conditions) and the formal loss of formic acid. As minor metabolites **8** and **9** were not sufficiently abundant for isolation and structural elucidation, their identification is based solely on accurate mass and the proposed mechanisms for their formation in Fig. 4.

To investigate the degradation of SphA (involving the proposed lactone-bridge cleavage depicted in Fig. 4), a series of stability studies of SphA were undertaken in MEM/DMSO (9 : 1) over a period of 48 h. Owing to the reactive α,β-unsaturated ketone present in SphA, and the various amino acids constituting the MEM cell medium, the formation of numerous SphA-amino acid adducts was anticipated.[28] Inspection of the total ion chromatograms acquired at different time intervals, revealed a substantial increase in SphA-derived components with time (Fig. 5). A closer comparison of the chromatogram of SphA and the blank sample acquired at 31 h incubation, emphasised the conversion of SphA into a plethora of degradation metabolites (Fig. S2 & 3†). However, the LC-MS data presented evidence for the formation of a major degradation metabolite **10** (*m/z* 317.1743, $C_{19}H_{25}O_4$) at 7.54 min, which increased in concentration as SphA decreased (Fig. 5). A more detailed inspection of the MS data for SphA and metabolite **10** is shown in Fig. S4, 5 and Table S2.† For SphA, in addition to the molecular ion $[M + H]^+$ (*m/z* 347) and the fragment ions $[M + H - H_2O]^+$ (*m/z* 329, base peak), $[M + H - CO_2 - H_2O]^+$ (*m/z* 285), ammonium $[M + NH_4]^+$ (*m/z* 364) and sodium $[M + Na]^+$ (*m/z* 369) adducts were detected. Similarly, the MS data of **10** showed the presence of several adducts including $[M + NH_4]^+$ (*m/z* 334), $[M + Na]^+$ (*m/z* 339) and $[M + K]^+$ (*m/z* 355), together with the protonated molecular ion $[M + H]^+$ (*m/z* 317, base peak) and a fragment ion at *m/z* 299 ($[M + H - H_2O]^+$). Interest towards major degradation metabolite **10** is revisited in a following section.

Proposed SphA degradation products-amino acid adducts

To get further insight into the instability of SphA in cell culture medium, simplified incubation media aimed at mimicking the MEM culture medium were envisaged. The resulting buffer medium therefore comprised an aqueous solution of HEPES, sodium hydrogen carbonate and monosodium phosphate prepared in the same composition as the culture medium. In this manner, the complexity of the LC-MS data was minimised, and the degradation metabolites could be analysed using a rational approach. Since no molecular ions matching SphA-amino acid adducts were identified during the former MEM incubation experiments, the strategy focused on first identifying possible SphA degradation products which could subsequently react with amino acids from the cell medium.

The investigation therefore initially involved analysis of SphA within a buffer-only solution (pH ~ 7.3), followed by several experiments whereby a specific amino acid was introduced individually to the medium (Fig. S6†).

The three SphA-derived metabolites **8** (*m/z* 301), **9** (*m/z* 285) and **10** (*m/z* 317) could all be located by mass extraction in the simplified LC-MS data obtained by this strategy (Table S3†). The remaining degradation products eluted at the reported retention times, possessing the respective molecular ions and formulas are reported in Table S3.† Having determined possible SphA **1** degradation products formed during incubation in the buffer-only solution, their reactivity towards various amino

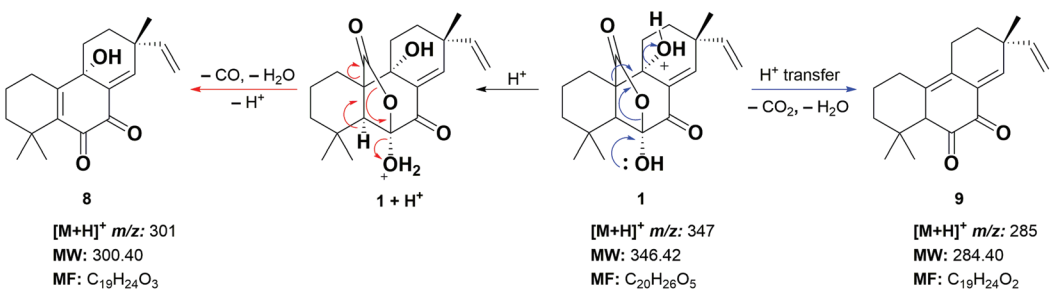

Fig. 4 Proposed chemical structures of minor SphA (**1**) degradation metabolites **8** and **9**. Possible degradation mechanisms involves lactone-bridge cleavage.

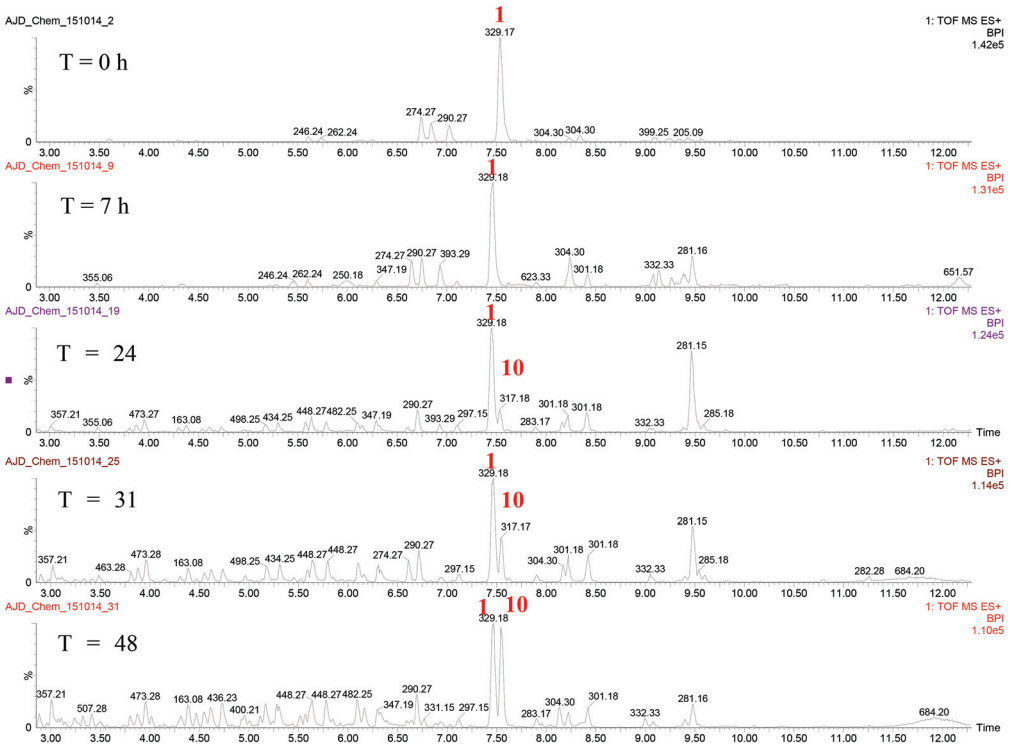

Fig. 5 Base peak ion chromatograms (ESI positive) of SphA incubated in MEM/DMSO (9 : 1) for t = 0, 7, 24, 31 and 48 h, highlighting the generation of major degradation metabolite **10**.

acids could be investigated more comprehensively. As expected, analysis of the different incubation experiments in the presence of amino acids verified the absence of SphA-amino acid adducts. However, inspection of the reactivity of SphA degradation products with amino acids revealed the generation of numerous possible adducts. These adducts were confirmed based solely on their detected molecular ions from the total ion chromatogram, as SphA degradation product (DP)-amino acid adducts were not abundant enough for isolation and structural elucidation.

The proposed SphA degradation product (DP)-amino acid adducts with their respective molecular ions and molecular formulas are reported in Table S4.† These adducts were comprised mainly of amino acids proposed to interact with the α,β-unsaturated ketone or carbonyl functionality of the SphA degradation products. The overall increased rate of degradation of SphA in the cell medium compared to the buffer solution (Fig. 2) may be ascribed to organocatalytic activity exhibited by the amino acids present in the cell medium.[29,30] The relevance of the amino acids on SphA stability was further supported by evaluation of the anti-cancer activity of SphA in either the absence or presence of 1 mM of *N*-acetyl-cysteine (NAC), a cysteine prodrug and glutathione precursor, added to the culture medium. The detailed IC_{50} values obtained by a 72 h drug exposure assay of two parental cancer cell lines (A2780, HCT116) and their sublines with acquired platinum drug resistance (cisplatin and oxaliplatin, respectively), showed that the presence of NAC resulted in an average 10× loss of SphA activity (Table 1). Additional studies are required to elucidate the exact structures and extent to which the amino acids facilitate the degradation of SphA. Interestingly, examination of the SphA DP-amino acid adducts (Table S4†) provided evidence for several adducts of the major degradation metabolite **10** (m/z 317). Furthermore, throughout the SphA incubation experiments, metabolite **10** was recognised as the predominant degradation component. Considering this observation, the next objective was aimed towards the further exploration of the major degradation metabolite **10**, denoted SphA-Met **10**.

Isolation and structural elucidation of major degradation metabolite SphA-Met 10

Since throughout the stability studies the concentration of SphA-Met **10** increased as SphA degraded over time, full conversion of SphA to SphA-Met **10** was established after prolonged incubation periods. To facilitate the isolation and purification of SphA-Met **10**, the degradation reaction was executed in the buffer-only solution rather than the more complex, faster degrading cell medium. Evaluation of the chromatogram acquired at 44 days of incubation in the buffer solution showed full conversion of SphA (m/z 329, $[M + H - H_2O]^+$) to SphA-Met **10** (m/z 317), along with minor metabolites detected at m/z 297, m/z 183 and m/z 163 (Fig. 6). The increase in concentration of component m/z 183 (4.65 min) from day 35 to 44, may be indicative of a degradation species with origin SphA-Met **10**. Once the incubation period was verified on an analytical scale, the degradation experiment was scaled-up

Table 1 Impact of NAC on the anticancer activity (IC_{50} values) of SphA in the ovarian cancer cell model A2780 and the colorectal cancer cell model HCT116 and the respective sublines with acquired cisplatin and oxaliplatin resistance. Cellular data values in table in μM. In the grey lanes, we report the IC_{50} ratio obtained by dividing the IC_{50} in presence of NAC by IC_{50} in the absence of NAC. The means of each row have also been calculated

	Condition/cell line	A2780	A2780/*cis* R	HCT116	HCT116 oxa R	Mean
	Cisplatin[a]	1.8	>10	—	—	—
	Oxaliplatin[a]	—	—	0.6	22	—
Exp 1	SphA	5	3	1	2	**2**
	SphA + 1 mM NAC	28	33	16	17	**24**
	IC_{50} ratio	6	12	15	10	**11**
Exp 2	SphA	2	2	3	2	**2**
	SphA + 1 mM NAC	19	17	36	15	**22**
	IC_{50} ratio	8	7	10	9	**9**
Mean ratio		7	10	13	9	**10**

[a] Reference IC_{50} values come from following published manuscript.[31]

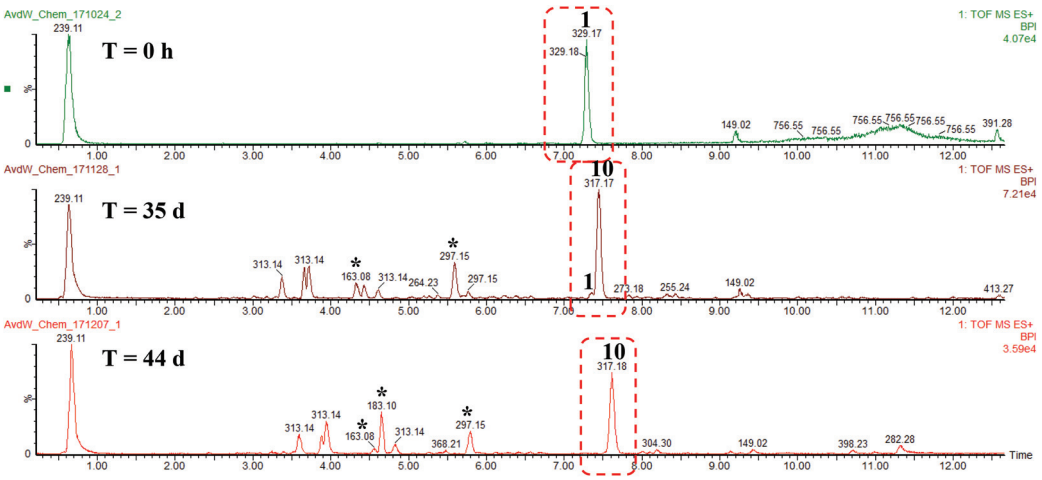

Fig. 6 Base peak ion chromatograms (ESI positive) of SphA (**1**) incubated in buffer/DMSO (9 : 1) for prolonged incubation periods (d = days) towards SphA-Met **10**. At t = 0 SphA (m/z 329.1750, $[M + H - H_2O]^+$) eluted at 7.29 min, whereas at t = 44 d of incubation SphA-Met **10** (m/z 317.1744, 7.61 min) is formed along with minor metabolites m/z 163.0757 (4.55 min), m/z 183.1017 (4.65 min) and m/z 297.1489 (5.79 min) indicated by *.

(20 mg SphA in buffer/DMSO, 9 mL : 1 mL) and the solution was incubated for 40 days. Optimal separation of the SphA-Met **10** from the crude mixture was then explored *via* an analytical HPLC system connected to a single quadrupole mass spectrometer. The isolation of **10** was finally executed employing preparative HPLC (C_{18} column) and UV detection (λ_{max} at 230 nm). The sample was introduced over seven manual injections, after which the isolates were collected manually. UV and MS chromatograms of the respective preparative and analytical separations acquired for isolation and purity determination are illustrated in Fig. S7–9.† Although the SphA degradation resulted in a low yield (2.9 mg, 16%) of metabolite **10**, it was obtained in excellent purity and deemed sufficient for NMR spectroscopy studies.

SphA-Met's **10** structural elucidation was embarked upon by implementing extensive 1D and 2D NMR measurements (COSY, HSQC, HMBC). The deciphering and analysis of the NMR spectral data proved to be challenging. This structural ambiguity was largely attributed to the high number of fully substituted carbons comprising part of the molecule, as well as detection difficulties of certain quaternary carbon signals (mass-limited sample). Nevertheless, the structure of SphA-Met **10** was successfully resolved by intensive exploration utilizing the HR-MS and NMR spectroscopy data, particularly utilizing varied acquisition parameters and pulse sequences for the latter.

The accurate mass of SphA-Met **10** (m/z 317.1753, $[M + H]^+$) corresponded to the molecular formula $C_{19}H_{24}O_4$ – equating to a loss of CH_2O (m/z 30) compared to SphA **1**. Thus, the initial speculation that SphA **1** had sustained a loss of two oxygen atoms through lactone bridge cleavage during the formation of **10**, in a similar manner to the proposed metabolites **8** and **9** (Fig. 4), demanded a re-evaluation. As such, the NMR spectra of SphA-Met **10** were closely scrutinised and compared to the reported SphA NMR spectroscopic signals as assigned by Evidente *et al.*[3,32] Direct comparison of SphA's ^1H and ^{13}C NMR spectroscopy signals to those detected for SphA-Met **10**, revealed structural similarities, as well as prominent differences. These distinct features are highlighted within the respective ^1H and ^{13}C NMR spectra (Fig. S10–13†). Essentially,

the ^{1}H, ^{13}C, APT, COSY and HSQC NMR spectra of **10**, supported the retention of the outer regions of the framework (blue carbon backbone) – *i.e.* rings **A** and **C** – of the parent compound **1**. On the other hand, the internal (red) ring **B** and lactone bridge appeared to have undergone structural modifications (Fig. 7). As this specific section of the molecule was proton-deficient in nature, long-range heteronuclear correlation data obtained from the HMBC NMR spectroscopy experiment proved crucial for the successful elucidation of the spiro-γ-lactone comprising metabolite **10**. The ^{1}H and ^{13}C NMR spectroscopic chemical shift assignments for SphA-Met **10** are presented in Table 2.

One of the primary obstacles we initially faced was that the ^{1}H and ^{13}C NMR spectral data showed fewer signals than expected from the molecular formula of $C_{19}H_{24}O_4$. The ^{13}C spectrum of **10** showed 17 signals that were assigned to **10** along with an aliphatic impurity at 29.85 ppm (Fig. S13†).[33] Thus, according to the MS data, two carbon signals could not be observed in the ^{13}C spectrum as a result of the mass-limited sample and/or the longer relaxation time experienced by quaternary carbons. Considering the reported carbon signals of SphA, vinyl carbons C_{15} (143.8 ppm) and C_{16} (114.3 ppm) of SphA-Met **10** were located at the same shift as those belonging to **1**. The α,β-unsaturated C_{14} was also identified at a similar shift (slightly more downfield), but it appeared as a broad signal. Another distinctive observation was the shift of C_9 from 71.1 ppm in SphA to 82.0 ppm in SphA-Met **10**. This effect could be explained by the substitution of the C_9 hydroxyl group with an ester carbonyl, forming the spiro-γ-lactone. Similarly, inspection of the ^{1}H NMR spectrum of SphA-Met **10**, in conjunction with SphA's spectrum, revealed vinyl protons H_{15} and $H_{16/16'}$ as a doublet of doublets (5.80 ppm) for H_{15}, along with two doublets ascribed to H_{16} (5.06 ppm) and $H_{16'}$ (5.11 ppm). Though shifted slightly more downfield, the signal of H_{14} was identified as a broad singlet at 7.20 ppm. Integration of the proton signals of SphA-Met **10** accounted for 23 protons, whereas a total of 24 protons was expected from the MS information. This absence was attributed to signal suppression of the carboxylic hydroxyl peak by proton exchange or peak broadening.

The COSY experiment revealed coupling interactions for the methylene protons H_{1-3}, $H_{11/12}$ and vinyl protons H_{16} and H_{15}

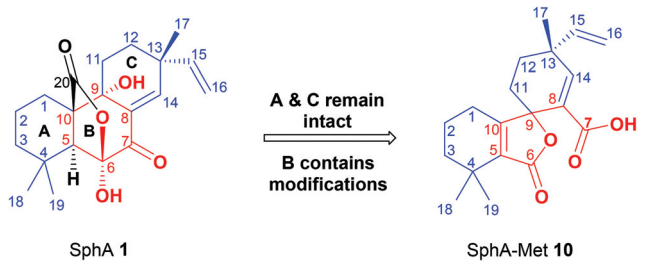

Fig. 7 Structural elucidation towards SphA-Met **10**. From the parent SphA compound the outer rings **A** and **C** were mainly retained, while ring **B** undergoes modification resulting in the structure of **10**.

Table 2 ^{1}H and ^{13}C data ($CDCl_3$) of SphA degradation metabolite (SphA-Met **10**). Chemical shifts reported in δ-values (ppm) from $CDCl_3$ reference

Atom (C)	$^{13}C^{a}$ δ (ppm)	$^{1}H^{a}$ δ (ppm)	HMBC ^{1}H–^{13}C (ppm)
1	24.0	2.03 [1.98–2.05], m, 1H	1.56 (3′)
1′		2.12 [2.09–2.18], m, 1H	
2	19.3	1.67 [1.62–1.70], m, 1H	2.12 (1′)
2′		1.75 [1.72–1.77], m, 1H	
3	38.8	1.46 [1.42–1.50], m, 1H	1.25 (18)
3′		1.56 [1.53–1.60], m, 1H	
4	30.8	—	1.20 (19), 1.25 (18), 1.56 (3′)
5	133.0	—	2.12 (1′), 1.20 (19), 1.25 (18), 1.56 (3′)
6	172.0	—	1.20 (19), 1.25 (18), 2.03 (1), 1.56 (3′)
7^{b}	169.5	—	7.20 (14)
8^{b}	125.6	—	7.20 (14), 1.82 (11), 1.94 (11′)
9	82.0	—	1.65 (12), 1.82 (11), 1.94 (11′/12′), 2.03 (1), 2.12 (1′)
10	164.3	—	2.12 (1′), 1.67 (2), 1.94 (11′)
11	31.7	1.82 [1.78–1.85], m, 1H	1.65 (12), 1.94 (12′)
11′		1.94 [1.89–1.98], m, 1H	
12	31.0	1.65 [1.62–1.70], m, 1H	1.20 (17), 5.80 (15)
12′		1.94 [1.89–1.98], m, 1H	
13	39.5	—	1.20 (17), 1.65 (12), 1.82 (11), 1.94 (11′/12′), 5.06 (16), 5.11 (16′), 5.80 (15)
14	156.0	7.20, br s, 1H	1.20 (17), 1.65 (12), 5.80 (15)
15	143.8	5.80, dd, 1H, J = 17.4, 10.5 Hz	1.20 (17), 1.65 (12), 1.94 (12′), 5.06 (16)
16	114.3	5.06, d, 1H, J = 17.4 Hz	
16′		5.11, d, 1H, J = 10.5 Hz	
17	25.1	1.20, s, 3H	1.65 (12), 1.94 (12′), 5.80 (15)
18^{c}	27.0	1.25, s, 3H	1.20 (19), 1.46 (3)
19^{c}	25.9	1.20, s, 3H	1.25 (18)

^{a} ^{1}H and ^{13}C signals assigned accordingly by implementing 2D ^{1}H, ^{1}H (COSY), 2D ^{13}C,^{1}H (HSQC, HMBC) and APT NMR spectroscopy. ^{b} ^{13}C NMR spectroscopy signal not visible in original ^{13}C NMR spectra, but identified from additional HMBC correlation cross-peaks. Assignments in red obtained from the additional HMBC correlation information (Fig. S22†). ^{c} ^{13}C and ^{1}H NMR spectroscopic signals of 18 and 19 are interchangeable.

(Fig. S14 and 15†). Furthermore, complete proton to carbon assignments were verified by inspection of the HSQC and HMBC spectra (Fig. S16–S18†). Overall, the ^{1}H NMR, ^{13}C NMR and APT spectral measurements of **10** identified three methyl groups, five methylene groups, one vinyl group, one trisubstituted alkene (methine group), one tetrasubstituted alkene, three quaternary carbon atoms and two carbonyl groups. Moreover, the IR spectrum of **10** revealed the key absorption bands of the γ-lactone at 1744 cm^{-1} and the α,β-unsaturated carboxylic acid at 1692 cm^{-1}.

In order to decipher the proton-deficient core of **10** the HMBC correlations were examined (Fig. S18–21†). The long-range ^{1}H–^{13}C NMR spectroscopic correlations are depicted as arrows in Fig. 8 and the precise assignments are reported in Table 2. The cross-peaks linking $H_{1'}$–C_5, $H_{3'}$–C_5, H_{18}/H_{19}–C_5 and H_{19}/H_{18}–C_5, as well as $H_{1'}$–C_{10}, confirmed the transformation of the formerly aliphatic C_5 and C_{10} into the tetrasubstituted olefinic carbons located at 133.0 ppm (C_5) and 164.3 ppm (C_{10}). The absence of the H_5 signal in the ^{1}H NMR spectrum of SphA-Met **10**, further supported this finding (Fig. S11†). Additionally, the presence of the quaternary C_9, connecting the spiro-constructed rings, was shown to correlate to the methylene protons of H_{11} and H_{12}. Another interesting validation of the structure from the HMBC spectrum was the correlation observed between H_{19}/H_{18}–C_6. The remaining interactions derived from the HMBC spectrum are depicted by the arrows in Fig. 8a and b. Since the carbon signals assigned to C_7 and C_8 were not detectable in the ^{13}C NMR spectrum at the low sample concentration, the application of a sensitivity enhanced and optimised NMR pulse sequence for long-range heteronuclear correlations was pursued.

Long-range heteronuclear single quantum multiple bond correlation (LR-HSQMBC) is a high-sensitivity pulse sequence capable of detecting $^{4,5}J_{CH}$ and $^{4,5}J_{NH}$ correlations with very small $^{n}J_{CH/NH}$ couplings (≤0.2 Hz for $^{n}J_{CH}$).[34] As such, LR-HSQMBC in combination with HMBC provide extremely valuable information to define structural elements having limited detectable protons.[35,36] By implementing LR-HSQMBC and optimised HMBC experiments ($^{n}J_{CH}$ = 3.5 Hz), additional long-range correlations were able to link the proton-containing portions of the outer rings to the proton-deficient core of SphA-Met **10**. These key heteronuclear correlations are illustrated by the arrows in Fig. 8c and further highlighted in Table 2. From the cross-peaks of H_{14}–C_7, H_{14}–C_8 and H_{11}–C_8, the carbon assignments of C_7 and C_8 could be identified at 169.5 ppm and 125.6 ppm, respectively. This completed the spectroscopic characterization of **10** and allowed the 2D structure to be unambiguously assigned. The specific HMBC NMR spectrum utilised in this study is illustrated in the ESI (Fig. S22†). Finally, with respect to structural elucidation, attempts to obtain a crystal structure and the optical rotation $[\alpha]_D$ proved to be ineffective due to the limited quantity of sample. However, SphA-Met **10** represents an unusual breakdown product of SphA (**1**) with a new structure that has not been previously described in the chemical literature.

Having successfully defined the molecular structure of SphA-Met **10**, by interpreting the synergistic data derived from the various NMR experiments, two potential degradation pathways were proposed. Interestingly, the hypothetical biosynthesis of SphA brings to mind the formation of the spirolactone norterpinoid aspergiloid I **11** (Scheme 1), as described by Guo *et al.*[37] These authors postulated that SphA would convert into aspergiloid E **12**, after which a "pimarane intermediate" **13** was accessible *via* hemiketal lactone ring-opening. The authors then postulated that aspergiloid I **11** could be formed from this "pimarane intermediate" **13** in a multi-step process (Scheme 1).

Considering the latter, potential intermediates of SphA (I, II and III) were first proposed which could undergo a loss of CH_2O (*m*/*z* 30) – matching the accurate mass and molecular formula of **10**. Ultimately, the envisioned degradation routes involved decarboxylation, oxidative cleavage and subsequent spiro-γ-lactone formation. The potential degradation steps are discussed in more detail within the scheme caption (Scheme 2).

The isolated metabolite **10** comprised a novel structure, yet two similar compounds have been identified in the literature. The isopimarane-type diterpene spiropolin A **14**, isolated from *Xylaria polymorpha*, includes a spiro-lactone structure resembling SphA-Met **10** (Fig. 9).[43] Notably, the oxidation of SphB **2** *via* sodium periodate led to the formation of semi-synthetic derivative **15** (Fig. 9).[9] The oxidised product **15** showed a

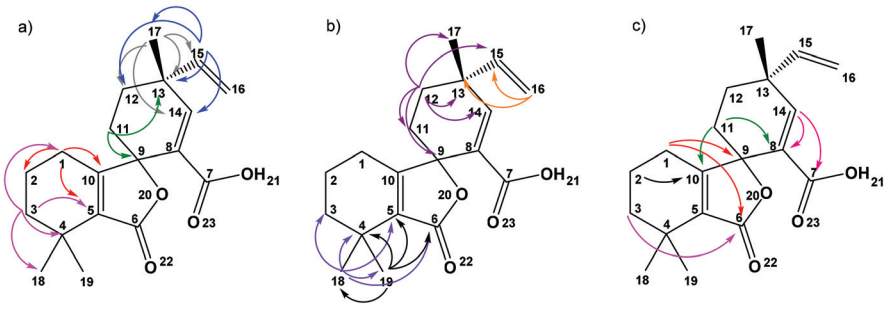

Fig. 8 Structural representation of SphA-Met **10** showing the key ^{1}H–^{13}C HMBC correlations observed when $^{n}J_{C,H}$ = 8.0 Hz for atoms (a) 1, 3, 11, 15, & 17 and (b) 12, 16, 18 & 19. (c) Additional HMBC ($^{n}J_{C,H}$ = 3.5 Hz) and LR-HSQMBC ($^{n}J_{C,H}$ = 2.0 Hz) correlations observed for atoms 1, 2, 3, 11 & 14, thus verifying the structure of **10** and chemical shifts of C_7 and C_8.

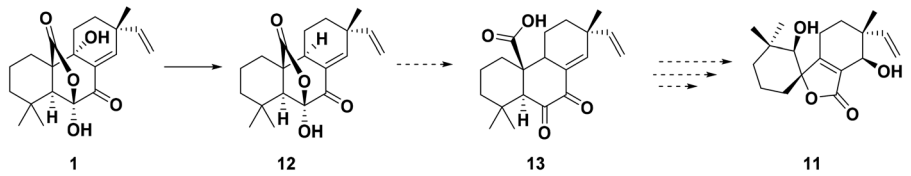

Scheme 1 Hypothetical biosynthetic scheme for the formation of Aspergiloid I **11** as proposed by Guo *et al.*[37] starting from SphA (**1**) and moving though aspergiloid E **12** and a "primarane intermediate" **13** before finally being converted into spirolactone aspergiloid I **11**.

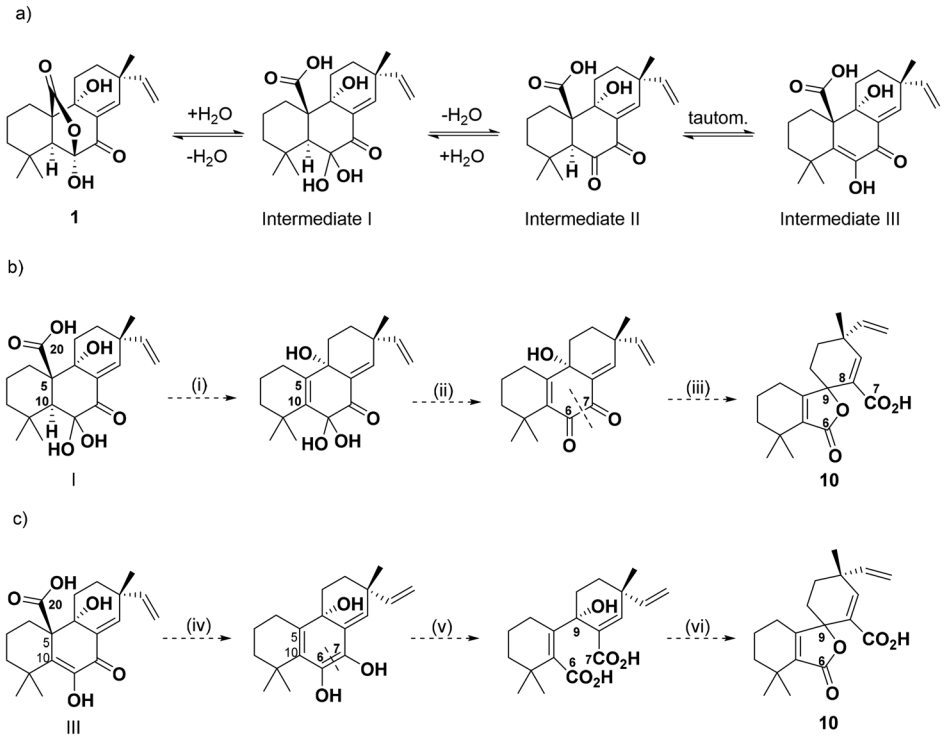

Scheme 2 Possible intermediate structures on degradation pathways from SphA (**1**) towards SphA-Met **10**. (a) Potential SphA (**1**) intermediates I, II and III following lactone bridge opening. (b) From intermediate I: (i) eliminative decarboxylation at C_{20}, (ii) hydrate-to-ketone conversion, (iii) oxidative cleavage at C_6/C_7 to carboxylic acid level (known to occur under chemical[38,39] and photochemical[40] conditions, and even with O_2)[41] and intramolecular esterification with C_9–OH to form the spiro-γ-lactone; (c) From intermediate III: (iv) decarboxylation at C_{20} and tautomerism, (v) oxidative cleavage of C_6/C_7 (this system is also tautomeric to the σ-hydroxy-ketone functional group arrangement for which chemical[38] and O_2 (in DMSO)[42] cleavage processes are known), (vi) addition of C_9–OH to C_6 (esterification) resulting in the formation of spiro-γ-lactone of **10**.

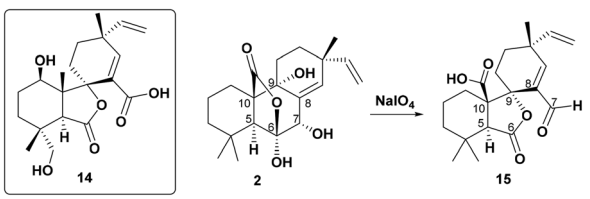

Fig. 9 Structural representation of spiropolin A **14** and the semi-synthetic derivative **15** synthesised from SphB **2**.

marked similarity to SphA-Met **10** – possessing a γ-lactone in place of ring B′ while retaining rings A′ and C′. Although the stereochemistry at C_9 of SphA-Met **10** could not be confirmed *via* the available NMR spectral data (the proton-deficient core of the molecule resulted in through-space experiments being inconclusive) and lack of a crystal structure, the α-configuration resembling the γ-lactone in **15** is quite probable. This assumption is based on mechanistic grounds of the proposed degradation pathway towards **10** (which involves interaction of the C_9-alcohol from the bottom face) and the direct comparison of structure **10** to that obtained by Evidente and co-workers during their oxidation of **2** into **15**.[9]

Disruption of the tricyclic pimarane system typically displayed by the sphaeropsidin analogues has generally resulted in greatly reduced phytotoxic and antimycotic activities, this also observed with their biogenically related aspergiloids.[9,37] Therefore, it was not surprising that a drastic loss in activity was observed for SphA-Met **10** in cellular assays against a panel of 6 cancer cell lines (Table 3). The poor growth inhibi-

Table 3 IC_{50} values determined by means of the colorimetric MTT assay after 72 h of exposure to the compound. Data represent the mean value of six replicates conducted once together. Cellular data values in table in μM

	A549	U373	HS683	MCF-7	SK-Mel-28	B16-F10	Mean ± SEM
Sph A **1**	7	5	5	7	3	3	5 ± 1
Sph A-Met **10**	>100	36	84	91	>100	51	>77 ± 11

tory activity displayed by SphA-Met **10** indicated that the major degradation metabolite of SphA does not contribute markedly to the promising antiproliferative behaviour of SphA. This result was in accordance with the previous study, which ascribed the potent anti-cancer activity (*via* rapid cellular shrinkage) to SphA itself, rather than its degradation metabolites.[12]

Conclusions

This study contributes to the understanding of SphA **1** instability in biological media. The degradation tendency of SphA appeared markedly enhanced in the presence of amino acids in comparison to aqueous buffers. Also of importance, was that the biological evaluation of aged SphA solutions and its major metabolite **10**, isolated and characterised in this study, indicate that the promising antiproliferative activity displayed by this fungal metabolite can be mainly attributed to its parent compound and not its degradation species. The two chemical properties of SphA investigated herein, *i.e.* its moderate water-solubility and poor stability in physiologic media, could therefore significantly limit its investigation *in vivo*. The poor stability of SphA, associated with the low antiproliferative properties of its metabolites, could thus mitigate its therapeutic potential. To overcome these limitations, the use of an advanced drug delivery system, such as liposomes, are currently of interest to us. Liposomes have been described to enhance drug solubility and protect encapsulated molecules from both chemical and enzymatic degradation.[44] Development and optimization of SphA-entrapped liposomes is thus ongoing in our research groups. The fact that SphA continues to exhibit remarkable anticancer activity, despite being susceptible to degradation, provides further impetus towards improving SphA's stability and delivery.

Experimental

Sphaeropsidin A

SphA was obtained from *Diplodia cupressi* grown *in vitro* and purified from the organic extract of the fungal culture filtrates as reported previously.[4] The purity >99% of the white crystals of SphA was ascertained by ^{1}H NMR, ESIMS and HPLC.

Determination of the solubility and stability of SphA in phosphate buffer

About 6 mg SphA was dispersed in 4 mL PBS pH 7.4 (Gibco, Life Technologies, Merelbeke, Belgium), stirred for 48 h at room temperature (20–22 °C) and filtrated through 0.22 μm pore size cellulose acetate syringe filters (VWR, Leuven, Belgium). The filtrate was analysed for its SphA content (see SphA assay) and diluted (dilution factor 5) in either PBS or MEM, and incubated under mild stirring at room temperature (20–22 °C) and at 37 °C. The incubated media were sampled at 24 and 48 h, diluted in the HPLC mobile phase and analysed for their SphA content (see SphA assay). Each condition was performed in three independent replicates.

High performance liquid chromatography quantification of SphA

SphA quantification was performed by means of an adaptation of the HPLC method described by Lallemand *et al.*[4] Briefly, the HPLC system (HP 1200 series, Agilent Technologies, Diegem, Belgium) was equipped with a quaternary pump, an autosampler, and a diode array detector. The separations were performed on a reverse-phase Hypersil Gold C-18 column (5 μm, 250 mm × 4.6 mm) (Thermo Fisher Scientific, Merelbeke, Belgium) at 30 °C. The mobile phase consisted of ultrapure water/methanol (70 : 30 v/v) acidified with 0.05% v/v trifluoroacetic acid (Sigma-Aldrich). The flow rate was 1.0 mL min^{-1}. The quantification was performed at 241 nm, the volume injected was 20 μL, and the analysis run time 10 min. All the samples were diluted in the mobile phase and kept at 4 °C until injection. A calibration curve in the mobile phase (2–200 μg mL^{-1}, determination coefficient $R^2 > 0.99$) was prepared daily and injected prior to sample analysis.

Cell culture

The mouse melanoma B16F10 (ATCC code CRL-6475) and the human melanoma SK-Mel-28 (ATCC code HTB-72) cell lines were obtained from the American Type Cell Culture Collection (ATCC, Manassas, VA, USA). Primary melanoma culture VM-21 and VM48 were obtained in Vienna and are characterised in the referenced publications.[45,46] The ovarian cancer cell model A2780 together with its cisplatin-resistant subline A2780/*cis* were obtained from Sigma-Aldrich. The colon cancer cell line HCT116 was obtained from ATCC (American Type Culture Collection). The oxaliplatin-resistant subline was established at the Institute of Cancer Research, Medical University Vienna, as published.[31] All cell lines, except the HCT116 model, were

cultured at 37 °C and 5% CO_2 in RPMI 1640 supplemented with 10% heat-inactivated fetal bovine serum and 2% L-glutamine (0.6 mg mL^{-1}). HCT116 was grown in ATCC-formulated McCoy's 5a Medium again with 10% heat-inactivated fetal bovine serum. For ATCC cell lines, the medium was supplemented with antibiotics (2% de penicillin/streptomycin (200 IU ml^{-1} and 200 μg mL^{-1}) and 0.1 mg mL^{-1} gentamicin).

MTT assay of SphA aged solution

To conduct the MTT assay in parallel to the SphA quantification study (Fig. 3), a stock solution of SphA at 0.3 mg mL^{-1} in RPMI 1640 culture medium (without DMSO) was prepared and stored at 37 °C. Samples of that stock solution were collected at different time points to prepare the SphA "aged" dilutions to be applied on cells for the MTT assay. Briefly, cells were seeded in 96 well plates 24 h prior to the exposure to SphA solutions. The latter were prepared by dilutions from the stock solution to get theoretical solutions ranging from 100 μM to 10 nM on the basis of the initial SphA concentration. Cells were then exposed to the SphA solutions for 72 h prior to residual viability assessment by MTT colorimetric method. The IC_{50} calculated corresponds thus to the theoretical SphA concentration that reduced by 50% the optical density in comparison to the untreated control cells. The actual remaining SphA concentration of the stock solution was quantified by HPLC as described above. Note that IC_{50} were not adjusted according to the remaining SphA concentration to highlight possible anti-cancer effects of "aged" SphA solution containing its various degradation species.

MTT assay with or without *N*-acetyl-cysteine

For combination experiments with NAC (*N*-acetylcysteine A7250, Sigma-Aldrich), A2780 and HCT116 cell models were seeded into 96-well plates and maintained for 24 h in the incubator. NAC was dissolved in PBS and added to the culture supernatant at a concentration of 1 mM for one h before addition of SphA at nine concentrations between 0.5 μM and 100 μM in triplicate. After 72 h co-incubation, cell viability was determined using an MTT-based cell viability assay (Easy4You, Biomedica, Vienna) following the instructions. IC_{50} values were calculated from dose–response curves using GraphPad Prism software.

Incubation conditions for SphA degradation analysis

SphA **1** (±1 mg, ~3 μmol) was dissolved in 100 μL DMSO and 900 μL Minimum Essential Medium (MEM) (HEPES modification, Sigma-Aldrich, M7278), and subsequently incubated at 37 °C. At different time intervals (t = 0, 7, 24, 31, 48 h...), 100 μL samples of the SphA **1** incubation mixture were collected, diluted with 900 μL mobile phase (0.1% formic acid/acetonitrile, 95 : 5), and injected for LC-MS analysis. Buffer solution (pH ~ 7.3) was prepared using 5.96 g L^{-1} HEPES (25 mM), 2.2 g L^{-1} $NaHCO_3$ (26 mM) and 0.122 NaH_2PO_4 (1 mM). The buffer incubation experiment was performed as described above, utilizing the buffer solution instead of the MEM cell medium. Amino acid (L-cystine·2 HCl, L-lysine·HCl, L-phenylalanine, L-leucine and L-tryptophan) solutions were prepared by dissolving ± 10 mg of each amino acid in 1 mL buffer solution (pH = 2.8–3.8). For the incubation experiment 900 μL of the amino acid solution was utilised instead of the MEM cell medium.

Liquid chromatography-mass spectrometry (LC-MS) analysis

LC-high resolution MS analysis was carried out utilizing a Waters Acquity ultra-performance liquid chromatograph (UPLC) (Waters, Milford, MA, USA) system with a binary solvent manager, sample manager, and column oven, interfaced through an electrospray ionization source to a Waters Synapt G2 quadruple time-of-flight (Q-TOF) mass spectrometer (Waters, Milford, MA, USA). The instrument was also connected to an Acquity photo diode array (PDA) detector. Electrospray ionization was utilised in positive mode with a cone voltage of 15 V. Nitrogen was used as the desolvation gas at 650 L h^{-1} and the desolvation temperature was set to 275 °C. Data were acquired by scanning from m/z 150 to m/z 1500 in resolution mode. In addition, MS^E fragmentation data were acquired using a collision energy ramp of 20–60 V. Chromatographic separation was achieved on a Acquity UPLC® BEH C18 1.7 μm, 2.1 × 100 mm column using a gradient mobile phase consisting of 0.1% formic acid in water (solvent A) and 0.1% formic acid in acetonitrile (solvent B). The mobile phase profile comprised a isocratic hold period (0.1 min) of 95% solvent A and 5% solvent B, followed by a linear gradient increase to 100% solvent B (12 min) and an equilibration step (1 min) of 95% solvent A and 5% solvent B. An injection volume of 7.5 μL was used. A flow rate of 0.4 mL min^{-1} was applied for a total run time of 15 min. MassLynx version 1.4 (Waters) was used for data acquisition and processing.

Each sample of incubated SphA **1** was analysed and scrutinised alongside a blank sample to account for compounds which were not attributed to SphA **1**, as well as the impurities from the laboratory equipment and instrumentation.

Incubation, isolation and purification of SphA-Met 10

SphA **1** (20.0 mg, 0.058 mmol) was dissolved in 1 mL DMSO and incubated in 9 mL buffer solution [25 mM HEPES, 26 mM $NaHCO_3$, 1 mM Na_2HPO_4 (pH 7.38), resembling buffer system of MEM] at 37 °C for 40 days. Upon full conversion of SphA **1** into SphA-Met **10**, the solution was purified *via* HPLC to afford SphA-Met **9** as an off-white solid (2.9 mg, 16%). HPLC separations were performed using an Agilent 1220 LC system (Agilent Technologies, Waldbronn, Germany) equipped with a dual channel gradient pump, manual injector, variable wavelength detector, and interfaced through an electrospray ionization source to an Agilent 6120B single quadrupole mass spectrometer. UV-Vis chromatograms were recorded at 230 nm. The system was controlled by Chemstation software (Agilent Technologies). Semi-preparative reversed phase LC separations were performed on a Phenomenex Gemini C_{18} column (250 × 10 mm i.d., 10 μm particles, Torrance, USA) using an injection volume of 1000–1500 μL. The mobile

phases utilised were methanol and 0.1% formic acid in water, with an isocratic composition of 35 : 65 (v/v%) for 22 minutes at a flow rate of 4.5 mL min^{-1}. Isolates were collected manually. Purity checks were performed on the same system using a Phenomenex Luna C_{18} column (150 × 2 mm i.d., 5 μm particles).

NMR spectroscopy

All NMR spectra were obtained at 25 °C, chemical shifts (δ) are reported in parts per million (ppm), multiplicities are indicated as s (singlet), d (doublet), dd (doublet of doublets), t (triplet), q (quartet), m (multiplet) and br s (broad singlet) and coupling constants (J) are expressed in Hertz (Hz).

Stellenbosch university. NMR spectra were recorded on a 600 MHz Varian Unity Inova (151 MHz for ^{13}C NMR spectra) at the Central Analytical Facilities (CAF) of Stellenbosch University. ^{1}H and ^{13}C spectra are referenced to the residual $CDCl_3$ solvent signal (δ_H 7.26 or δ_C 77.16 ppm). NMR spectra were processed using MestReNova version 11.0.3-18688.

NCI. NMR spectra were recorded on an Avance III NMR spectrometer equipped with a 3 mm cryogenic probe and operating at 600 MHz for ^{1}H and 150 MHz for ^{13}C. Spectra were calibrated to residual solvent signals at δ_H 7.24 and δ_C 77.2 ($CDCl_3$). All 2D NMR experiments were acquired with nonuniform sampling (NUS) set to 25%. HMBC experiments were run with $^{n}J_{CH}$ = 8.3 or 3.5 Hz, and the LR-HSQMBC experiment was optimized for $^{n}J_{CH}$ = 2.0 Hz.

Spectroscopic characterization of SphA-Met 10, (4*R*)-4,4′,4′-trimethyl-3′-oxo-4-vinyl-4′,5′,6′,7′-tetrahydro-3′*H*-spiro[cyclohexane-1,1′-isobenzofuran]-2-ene-2-carboxylic acid

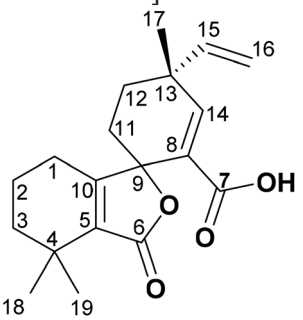

IR (ATR) cm^{-1}. 3155 (s, O–H str), 3019 (m, alkane), 2981, 2254, 1795, 1744 (s, γ-lactone), 1692 (s, α, β-unsaturated carboxylic acid), 1658 (m, cyclic alkene), 1468, 1380, 1262, 1216, 1167, 1095; **^{1}H NMR (600 MHz, $CDCl_3$) δ** 7.20 (br s, 1H, H_{14}), 5.80 (dd, J = 17.4, 10.5 Hz, 1H, H_{15}), 5.11 (d, J = 10.5 Hz, 1H, $H_{16'}$), 5.06 (d, J = 17.4 Hz, 1H, H_{16}), 1.98–1.89 (m, 2H, $H_{11'}$, $H_{12'}$), 1.85–1.78 (m, 1H, H_{11}), 1.70–1.62 (m, 1H, H_{12}), 2.18–2.09 (m, 1H, $H_{1'}$), 2.05–1.98 (m, 1H, H_1), 1.77–1.72 (m, 1H, $H_{2'}$), 1.70–1.62 (m, 1H, H_2), 1.60–1.53 (m, 1H, $H_{3'}$), 1.50–1.42 (m, 1H, H_3), 1.25 (s, 3H, H_{18}/H_{19}), 1.20 (s, 6H, H_{17}, H_{19}/H_{18}); **^{13}C NMR (151 MHz, $CDCl_3$) δ** 172.0 (s, C_6), 169.5 (s, C_7), 164.3 (s, C_{10}), 156.0 (d, C_{14}), 143.8 (d, C_{15}), 133.0 (s, C_5), 125.6 (s, C_8), 114.3 (t, C_{16}), 82.0 (s, C_9), 39.5 (s, C_{13}), 38.8 (t, C_3), 31.7 (t, C_{11}), 31.0 (t, C_{12}), 30.8 (s, C_4), 27.0 (q, C_{18}/C_{19}), 25.9 (q, C_{19}/C_{18}), 25.1 (q, C_{17}), 24.0 (t, C_1), 19.3 (t, C_2); **HRMS m/z** ESI^+ calculated for $C_{19}H_{24}O_4$ $[M + H]^+$ 317.1753, found 317.1743.

Author contribution

Prof. Willem A. L. van Otterlo – primary chemistry oversight; Dr Alet E. van der Westhuyzen – SphA degradation studies, metabolite isolation, HRMS work, characterization; Prof. André de Villiers – MS specialist, HPLC prep isolation; Retired Prof. Ivan R. Green – natural products chemistry, isolation and spectroscopic characterization; Prof. Veronique Mathieu – primary oversight on antiproliferative studies; Dr Aude Ingels – antiproliferation studies; Mr Rémi Rosière & Mr Karim Amighi –SphA degradation studies and degradation-HRMS studies; Dr Lukas Oberer – natural product characterisation and modelling of spectroscopic results. Ms van der Westhuyzen interacted with Dr Oberer while on a 3 month research internship at Novartis, Basel. Also provided assistance in possible metabolite formation bio-synthetic pathways; Dr Kirk R. Gustafson & Dr Dongdong Wang – performed long-distance NMR spectroscopy studies on the SphA metabolite and provided assistance in terms of confirming structural analysis through long-range NMR spectroscopic experiments; Dr Lucia Maddau - Fungal production of metabolite sphaeropsidin A; Prof. Antonio Evidente & Dr Marco Masi –isolation and purification of sphaeropsidin A; Prof. Walter Berger – performed *N*-acetylcysteine (NAC)-based experiments on cell lines with and without resistance mechanisms; Prof. Alexander Kornienko – Prof. Alexander Kornienko made a number of intellectual contributions to the design and conclusions of the proposed work, specifically in terms of mechanisms for possible formation of SphA metabolites.

Conflicts of interest

There are no conflicts of interest to declare.

Acknowledgements

WALvO, AvdW, AdV and IRG thank the National Research Foundation (NRF, Grant UIDs 93528, 109465 and 113322), South Africa for research funding and the Faculty of Science, Stellenbosch University for research support. These authors would also like to thank Dr J. Brand for NMR spectroscopic experiments (SU) and Dr M.A. Stander for assistance with the LC-HR-MS analyses, both from Central Analytical Facilities (CAF), Stellenbosch, and Ms E.N. Uushona for assistance with the preparative isolation of compound **10** with research support from AdV's NRF grants (UIDs 98897 and 118530). AvdW would also like to thank Prof B. Klumperman (co-supervisor, Stellenbosch University) for funding support through the South African Research Chairs Initiative of the Department of Science and Technology (DST) and NRF of South Africa (Grant No 46855). AK is grateful to the National Institutes of

Health (grants 1R15CA227680-01A1 and 1R21GM131717-01), and AE is associated with the Istituto di Chimica Biomolecolare del CNR, Pozzuoli, Italy.

References

1 M. Masi, L. Maddau, B. T. Linaldeddu, B. Scanu, A. Evidente and A. Cimmino, *Curr. Med. Chem.*, 2018, **25**, 208–252.
2 P. Reveglia, A. Cimmino, M. Masi, P. Nocera, N. Berova, G. Ellestad and A. Evidente, *Chirality*, 2018, **30**, 1115–1134.
3 A. Evidente, L. Sparapano, A. Motta, F. Giordano, O. Fierro and S. Frisullo, *Phytochemistry*, 1996, **42**, 1541–1546.
4 B. Lallemand, M. Masi, L. Maddau, M. De Lorenzi, R. Dam, A. Cimmino, L. Moreno y Banuls, A. Andolfi, R. Kiss, V. Mathieu and A. Evidente, *Phytochem. Lett.*, 2012, **5**, 770–775.
5 A. Cimmino, L. Maddau, M. Masi, M. Evidente, B. T. Linaldeddu and A. Evidente, *Tetrahedron*, 2016, **72**, 6788–6793.
6 A. Andolfi, L. Maddau, S. Basso, B. T. Linaldeddu, A. Cimmino, B. Scanu, A. Deidda, A. Tuzi and A. Evidente, *J. Nat. Prod.*, 2014, **77**, 2352–2360.
7 M. Masi, L. Maddau, B. T. Linaldeddu, A. Cimmino, W. D'Amico, B. Scanu, M. Evidente, A. Tuzi and A. Evidente, *J. Agric. Food Chem.*, 2016, **64**, 217–225.
8 Y. Li, R. Scott, A. R. Hooper, G. A. Bartholomeusz, A. Kornienko and G. F. Bills, *Bioorg. Med. Chem. Lett.*, 2017, **27**, 5436–5440.
9 L. Sparapano, G. Bruno, O. Fierro and A. Evidente, *Phytochemistry*, 2004, **65**, 189–198.
10 A. Evidente, V. Venturi, M. Masi, G. Degrassi, A. Cimmino, L. Maddau and A. Andolfi, *J. Nat. Prod.*, 2011, **74**, 2520–2525.
11 A. Cimmino, A. Andolfi, F. Avolio, A. Ali, N. Tabanca, I. A. Khan and A. Evidente, *Chem. Biodiversity*, 2013, **10**, 1239–1251.
12 V. Mathieu, A. Chantôme, F. Lefranc, A. Cimmino, W. Miklos, V. Paulitschke, T. Mohr, L. Maddau, A. Kornienko, W. Berger, C. Vandier, A. Evidente, E. Delpire and R. Kiss, *Cell. Mol. Life Sci.*, 2015, **72**, 3731–3746.
13 M. M. Gottesman, *Annu. Rev. Med.*, 2002, **53**, 615–627.
14 G. Szakács, J. K. Paterson, J. A. Ludwig, C. Booth-Genthe and M. M. Gottesman, *Nat. Rev. Drug Discovery*, 2006, **5**, 219–234.
15 F. H. Igney and P. H. Krammer, *Nat. Rev. Cancer*, 2002, **2**, 277–288.
16 B. Mansoori, A. Mohammadi, S. Davudian, S. Shirjang and B. Baradaran, *Adv. Pharm. Bull.*, 2017, **7**, 339–348.
17 X. Wang, H. Zhang and X. Chen, *Cancer Drug Resist.*, 2019, **2**, 141–160.
18 J. F. R. Kerr, C. M. Winterford and B. V. Harmon, *Cancer*, 1994, **73**, 2013–2026.
19 S. H. Kaufmann and W. C. Earnshaw, *Exp. Cell Res.*, 2000, **256**, 42–49.
20 J. L. Koff, S. Ramachandiran and L. Bernal-Mizrachi, *Int. J. Mol. Sci.*, 2015, **16**, 2942–2955.
21 X.-N. Wang, B. P. Bashyal, E. M. K. Wijeratne, J. M. U'Ren, M. X. Liu, M. K. Gunatilaka, A. E. Arnold and A. A. L. Gunatilaka, *J. Nat. Prod.*, 2011, **74**, 2052–2061.
22 A. Ingels, C. Dinhof, A. D. Garg, L. Maddau, M. Masi, A. Evidente, W. Berger, B. Dejaegher and V. Mathieu, *Cancer Chemother. Pharmacol.*, 2017, **79**, 971–983.
23 G. L. Amidon, H. Lennernäs, V. P. Shah and J. R. Crison, *Pharm. Res.*, 1995, **12**, 413–420.
24 C. A. Lipinski, F. Lombardo, B. W. Dominy and P. J. Feeney, *Adv. Drug Delivery Rev.*, 2001, **46**, 3–26.
25 A. P. Hill and R. J. Young, *Drug Discovery Today*, 2010, **15**, 648–655.
26 M. A. Walker, *Bioorg. Med. Chem. Lett.*, 2017, **27**, 5100–5108.
27 D. P. Demarque, A. E. M. Crotti, R. Vessecchi, J. L. C. Lopes and N. P. Lopes, *Nat. Prod. Rep.*, 2016, **33**, 432–455.
28 R. A. Bauer, *Drug Discovery Today*, 2015, **20**, 1061–1073.
29 L.-W. Xu and Y. Lu, *Org. Biomol. Chem.*, 2008, **6**, 2047–2053.
30 M. P. van der Helm, B. Klemm and R. Eelkema, *Nat. Rev. Chem.*, 2019, **3**, 491–508.
31 S. A. Abramkin, U. Jungwirth, S. M. Valiahdi, C. Dworak, L. Habala, K. Meelich, W. Berger, M. A. Jakupec, C. G. Hartinger, A. A. Nazarov, M. Galanski and B. K. Keppler, *J. Med. Chem.*, 2010, **53**, 7356–7364.
32 M. Masi, A. Cimmino, L. Maddau, A. Kornienko, A. Tuzi and A. Evidente, *Tetrahedron Lett.*, 2016, **57**, 4592–4594.
33 H. E. Gottlieb, V. Kotlyar and A. Nudelman, *J. Org. Chem.*, 1997, **62**, 7512–7515.
34 R. T. Williamson, A. V. Buevich, G. E. Martin and T. Parella, *J. Org. Chem.*, 2014, **79**, 3887–3894.
35 S. T. S. Chan, R. R. Nani, E. A. Schauer, G. E. Martin, R. T. Williamson, J. Saurí, A. V. Buevich, W. A. Schafer, L. A. Joyce, A. K. L. Goey, W. D. Figg, T. T. Ransom, C. J. Henrich, T. C. McKee, A. Moser, S. A. MacDonald, S. Khan, J. B. McMahon, M. J. Schnermann and K. R. Gustafson, *J. Org. Chem.*, 2016, **81**, 10631–10640.
36 D. J. Milanowski, N. Oku, L. K. Cartner, H. R. Bokesch, R. T. Williamson, J. Sauri, Y. Z. Liu, K. A. Blinov, Y. Q. Ding, X. C. Li, D. Ferreira, L. A. Walker, S. Khan, M. T. Davies-Coleman, J. A. Kelley, J. B. McMahon, G. E. Martin and K. R. Gustafson, *Chem. Sci.*, 2018, **9**, 307–314.
37 Z. K. Guo, R. Wang, W. Huang, X. N. Li, R. Jiang, R. X. Tan and H. M. Ge, *Beilstein J. Org. Chem.*, 2014, **10**, 2677–2682.
38 S. O. Nwaukwa and P. M. Keehn, *Tetrahedron Lett.*, 1982, **23**, 3135–3138.
39 S. M. Kim, H. S. Yoo, H. Hosono, J. W. Yang and S. W. Kim, *Sci. Rep.*, 2015, **5**, 10366.
40 P. Sivaguru, Z. Wang, G. Zanoni and X. Bi, *Chem. Soc. Rev.*, 2019, **48**, 2615–2656.
41 S. Gundala, C. L. Fagan, E. G. Delany and S. J. Connon, *Synlett*, 2013, **24**, 1225–1228.
42 G. Speier and Z. Tyeklár, *J. Mol. Catal.*, 1990, **57**, L17–L19.
43 Y. Shiono, N. Matsui, T. Imaizumi, T. Koseki, T. Murayama, E. Kwon, T. Abe and K.-i. Kimura, *Phytochem. Lett.*, 2013, **6**, 439–443.

44 G. Bozzuto and A. Molinari, *Int. J. Nanomed.*, 2015, **10**, 975–999.
45 W. Berger, E. Hauptmann, L. Elbling, M. Vetterlein, E. M. Kokoschka and M. Micksche, *Int. J. Cancer*, 1997, **71**, 108–115.
46 P. Birner, A. S. Berghoff, C. Dinhof, C. Pirker, D. Capper, S. F. Schoppmann, P. Petzelbauer, A. von Deimling, W. Berger and M. Preusser, *Arch. Dermatol. Res.*, 2014, **306**, 873–884.